

Geophysical Research Letters[®]



RESEARCH LETTER

10.1029/2023GL106282

Direct Detection of Ongoing Magnetic Reconnection at Mercury's High-Latitude Magnetopause

Key Points:

- A reconnection X-line region is first observed in the Mercury's magnetopause during the northward interplanetary magnetic field
- The small-scale magnetic flux ropes in the X-line region could be the seed of the flux transfer event shower
- The flux ropes probably expand and is deflected after they are ejected away from the X-line region

Rongsheng Wang^{1,2,3} , Zihang Cheng^{2,3} , James A. Slavin⁴ , Quanming Lu^{1,2,3} , Jim Raines⁴ , San Lu^{1,2,3} , Jin Guo^{2,3} , and Walter Gonzalez⁵ 

¹Deep Space Exploration Laboratory, Hefei, China, ²CAS Center for Excellence in Comparative Planetology/CAS Key Laboratory of Geospace Environment/Anhui Mengcheng National Geophysical Observatory, University of Science and Technology of China, Hefei, China, ³Collaborative Innovation Center of Astronautical Science and Technology, Harbin, China, ⁴Department of Climate and Space Sciences and Engineering, University of Michigan, Ann Arbor, MI, USA, ⁵China-Brazil Joint Laboratory for Space Weather, Instituto Nacional de Pesquisas Espaciais, São Jose dos Campos, Brazil

Correspondence to:

R. Wang,
rswan@ustc.edu.cn

Citation:

Wang, R., Cheng, Z., Slavin, J. A., Lu, Q., Raines, J., Lu, S., et al. (2024). Direct detection of ongoing magnetic reconnection at Mercury's high-latitude magnetopause. *Geophysical Research Letters*, 51, e2023GL106282. <https://doi.org/10.1029/2023GL106282>

Received 23 OCT 2023

Accepted 12 FEB 2024

Author Contributions:

Conceptualization: Rongsheng Wang

Formal analysis: Rongsheng Wang

Investigation: Rongsheng Wang, Zihang Cheng

Software: Zihang Cheng

Supervision: Rongsheng Wang

Writing – original draft:

Rongsheng Wang, Zihang Cheng

Writing – review & editing: James

A. Slavin, Quanming Lu

Abstract An ongoing magnetic reconnection event was detected in the Mercury's high latitude magnetopause during a northward interplanetary magnetic field. The reconnection X-line region was revealed in the Mercury's magnetopause based on the encountered flux ropes ejected away from this region both planetward and tailward. A series of magnetic flux ropes, known as flux transfer event shower were observed tailward of this X-line region. These flux ropes were probably expanding and deflected as they were ejected away tailward from the X-line region. Large-amplitude variations in all three components of the magnetic field and a few small-scale flux ropes were observed inside the X-line region, which could be the seed of the flux rope shower at the magnetopause. The observations suggest that magnetic reconnection is highly dynamic and persistent in Mercury's magnetosphere.

Plain Language Summary Magnetic reconnection has been regarded as the most important process for dynamics of the Mercury's magnetosphere and for the interaction between the solar wind and the Mercury's magnetosphere also. Although magnetic flux ropes and flux transfer events (FTEs) resulting from magnetic reconnection have been extensively observed in the Mercury's magnetosphere, the key region of magnetic reconnection, namely the X-line region, has never been reported so far by the spacecraft. Here, we present the first evidence of the reconnection X-line region in the Mercury's magnetosphere. A few small-scale magnetic flux ropes are observed inside the reconnection X-line region, which could be the seed of the observed magnetic FTE shower. Furthermore, the evolution of these flux ropes is addressed also based on the spacecraft observations.

1. Introduction

The intrinsic magnetic field of Mercury is the dipolar magnetic field aligned with the rotation axis and has the same polarity as the Earth's. However, the field strength at Mercury's surface in the magnetic equatorial plane is only ~1% of the Earth's field (Alexeev et al., 2010; B. J. Anderson et al., 2008, 2011). In the proximity of Mercury, the interplanetary magnetic field (IMF) intensity and the solar wind density are generally much higher than those at the Earth (Slavin & Holzer, 1979; Sun et al., 2022). Therefore, Mercury's magnetosphere can be strongly driven by the solar wind. It has been found recently that the interaction between Mercury's magnetosphere and the solar wind is controlled primarily by magnetic reconnection, during which magnetic topology is re-configured and stored magnetic energy is rapidly released (e.g., DiBraccio et al., 2015; Imber et al., 2014; Slavin et al., 2010; Sun et al., 2015; Sun, Slavin, Smith, et al., 2020; J. Zhong, Lee, et al., 2020).

Under the condition of the southwardly directed IMF, reconnection occurs at the magnetopause sub-solar point, and the reconnected magnetic fluxes are transferred tailward, added temporally to the magnetotail, and finally released again by the magnetotail reconnection (Russell & Elphic, 1978; Slavin et al., 2010; Sun, Slavin, Dewey, et al., 2020). Evidence for magnetic reconnection has been extensively observed in Mercury's magnetosphere, including flux transfer events (FTEs) or magnetic flux ropes at the magnetopause (e.g., Imber et al., 2014; Slavin et al., 2010; Sun, Slavin, Smith, et al., 2020; J. Zhong, Wei, et al., 2020) as well as magnetic flux ropes, magnetic islands, or traveling compression regions in the magnetotail (DiBraccio et al., 2015; Slavin, Anderson, et al., 2012; J. Zhong et al., 2018; Z. H. Zhong et al., 2018; J. Zhong, Lee, et al., 2020; Sun, Slavin, Smith, et al., 2020). The flux ropes in Mercury's magnetosphere are detected commonly in series, named FTE or flux

© 2024. The Authors.

This is an open access article under the terms of the [Creative Commons Attribution-NonCommercial-NoDerivs License](#), which permits use and distribution in any medium, provided the original work is properly cited, the use is non-commercial and no modifications or adaptations are made.

rope shower (Slavin, Imber, et al., 2012; Sun, Slavin, Smith, et al., 2020; J. Zhong, Wei, et al., 2020), more often than that in the Earth's magnetosphere where the FTEs or magnetic flux ropes are observed occasionally in a train as well (e.g., Chen et al., 2008; Guo et al., 2021; Lee & Fu, 1985; Rijnbeek et al., 1984; Russell & Elphic, 1978; Wang et al., 2012, 2016). The flux rope shower is assumed to be generated by the multiple reconnection X-line model where magnetic reconnection occurs simultaneously at multiple points and thus the flux rope is naturally produced between any two adjacent reconnection X-lines (Imber et al., 2014; Sun, Slavin, Smith, et al., 2020; J. Zhong, Wei, et al., 2020). Alternatively, the flux rope shower could be generated also during a turbulent magnetic reconnection during which many secondary flux ropes are created in the X-line region and then ejected away, as observed in the Earth's magnetosphere (e.g., Lu, Fu, et al., 2022; Wang et al., 2016). The electric field in the X-line region was inferred according to the observations in the polar cap boundary (PCB) (Gershman et al., 2016) and the reconnection Hall magnetic field was detected directly (Sun, Slavin, Dewey, et al., 2020). However, the reconnection X-line region in the Mercury's magnetosphere has not been sufficiently investigated.

The coupling between the solar wind and Mercury's magnetosphere during a southward IMF has been revealed by numerical simulations (e.g., Jia et al., 2019; Lu, Guo, et al., 2022) and observations (Slavin, Imber, et al., 2012; Sun, Slavin, Smith, et al., 2020; J. Zhong, Wei, et al., 2020). However, the dynamics of Mercury's magnetosphere and the interaction between the solar wind and the magnetosphere under the condition of the northward directed IMF have rarely been investigated with spacecraft data (Slavin, Imber, et al., 2012). Only recently, the FTEs during the northward IMF on Mercury's dayside magnetopause were discussed (e.g., Slavin et al., 2014; Sun et al., 2022; Zomerdijk-Russell et al., 2023). Moreover, the coupling in the northward IMF was simulated recently by a three-dimensional hybrid simulation (Lu, Guo, et al., 2022).

In this letter, we report one reconnection event observed by the MErcury Surface Space ENvironment, GEochemistry, and Ranging (MESSENGER) spacecraft at the nightside magnetopause, when the IMF pointed north. The MESSENGER spacecraft directly passed through the reconnection X-line region from one exhaust to the other and detected many magnetic flux ropes not only in both exhausts but also in the X-line region. The formation mechanism, evolution, and implication of these flux ropes in the Mercury's nightside magnetopause are addressed.

2. Observation and Analysis

In this paper, the magnetic field data and ion differential energy flux data are obtained from the instruments of Magnetometer (MAG) (Anderson et al., 2007), and the Fast Imaging Plasma Spectrometer (FIPS) (Andrews et al., 2007) onboard the MESSENGER spacecraft, respectively. FIPS is a time-of-flight (TOF) mass spectrometer measuring the mass-per-charge (m/q) and energy-per-charge (E/q) ratios of incident ions. Due to the mission's thermal design, the direct line of sight of FIPS in the solar direction is partially obstructed by the MESSENGER spacecraft sunshade and other parts of the structure (e.g., Gershman et al., 2012). Hence, the instantaneous field-of-view (FOV) is approximately 1.15π sr. Because the solid angle detected by FIPS is less than one third of the ideal 4π sr, an inversion method to recover moment estimates from partially observed distributions was used to get the plasma density and temperature (e.g., Gershman et al., 2013).

On 9 April 2011, the MESSENGER spacecraft was located in the solar wind for more than 2 hr since $\sim 01:00$ UT and then crossed the bow shock (Figure 1) as well as the Mercury's magnetosphere. The magnetic field and plasma data in this interval are displayed (Figure 1) in the Mercury Solar-Magnetospheric (MSM) coordinate system, where x is anti-parallel to solar wind velocity, z is normal to Mercury's orbital plane and points northward ($\sim 0.2R_M$ northward of the planetary center on the rotation axis), and y completes the right-handed system. In the solar wind, the magnetic field magnitude was nearly constant (~ 26 nT, Figure 1f), B_z was positive except for a very short excursion into the negative dip at $\sim 01:56$ UT (Figure 1e), B_y was always positive and kept a relatively high value (~ 20 nT) and B_x fluctuated around 0 (Figure 1a). The observations indicate that the IMF was stable and almost northward during the time interval.

Later, the MESSENGER spacecraft passed through the southern magnetopause at $(-1.7, 0.3, -2.4)R_M$ during 04:48–04:58 UT, in the near-midnight sector of the Mercury's magnetopause, as schematized in Figure 2. An overview of this magnetopause crossing is shown in Figure 3. In this crossing, the spacecraft encountered the current sheet center multiple times, namely B_x changed sign, for example, at $\sim 04:52$, $\sim 04:53:40$, and $\sim 04:54:10$ UT (Figure 3a). The repeated encounters of the current sheet center allow us to investigate the physics processes inside the current sheet. B_x was initially ~ -60 nT and then gradually increased to 0 at $\sim 04:52$ UT, with many

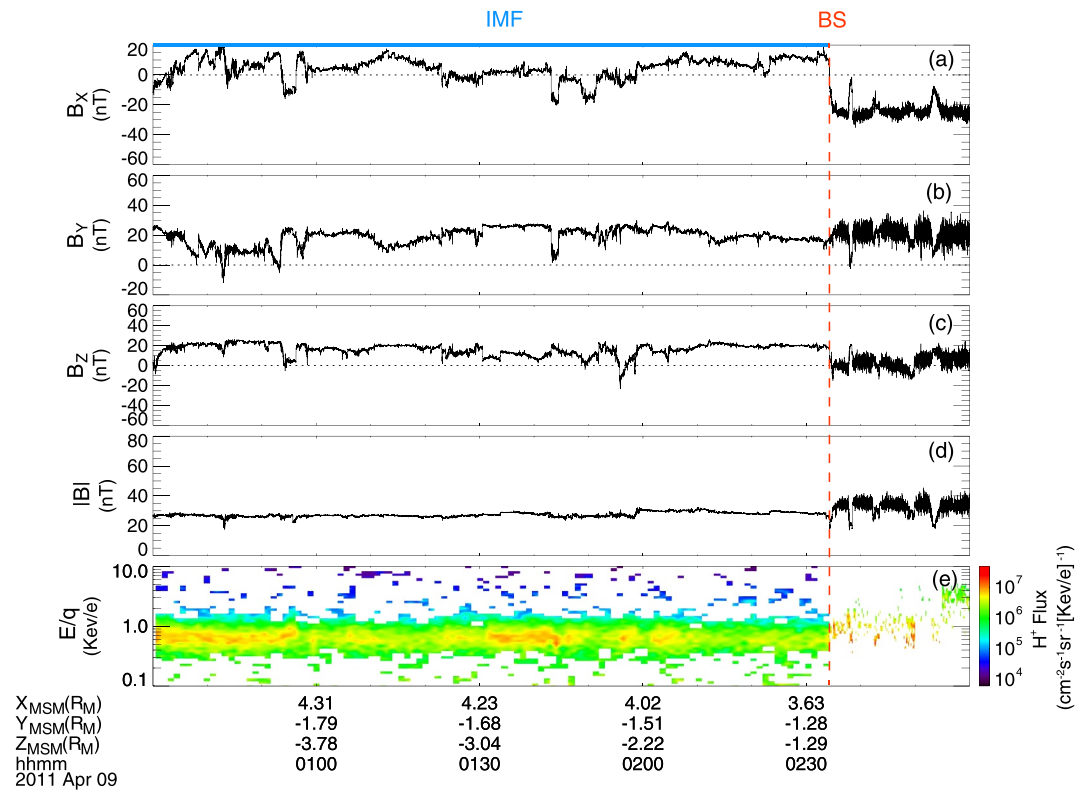


Figure 1. The interplanetary magnetic field condition before MErcury Surface Space ENvironment, GEOchemistry, and Ranging's magnetopause current sheet crossing. The red dashed line denotes the bow shock. (a–d) Magnetic field data (20 samples s^{-1}) in the Mercury Solar-Magnetospheric coordinate system. (e) Spectrogram of the proton differential energy flux versus energy per charge and time ($cm^{-2} Sr^{-2} S^{-1} [KeV/e]^{-1}$).

sharp peaks. Afterward, B_x fluctuated around 0 for ~ 1.5 min (04:52:00–04:53:35 UT), then became -60 nT for a short while (04:53:35–04:54:00 UT), changed sign sharply at $\sim 04:54:10$ UT and finally kept around 10 nT with many small peaks as well as valleys after 04:54:10 UT. After this magnetopause crossing, the northward magnetic field was persistently observed for more than 20 min (not shown). Thus, it is assumed that the IMF was northward during the magnetopause crossing.

The proton energy spectrum displayed a clear difference before and after 04:54:14 UT when B_x roughly reversed from negative to positive. After this time, the proton shows high fluxes at the energy range of ~ 0.4 – 2 keV (Figure 3e), and the number density was about $30 cm^{-3}$ (black trace in Figure 3g). In contrast, the proton energy spectrum shows much lower fluxes prior to 04:54:14 UT even if the spacecraft was near the current sheet center ($|B_x| < 10$ nT), with a few local flux enhancements, for example, at $\sim 04:49:24$, $\sim 04:51:55$, $\sim 04:53:40$ UT. Thus, the number density was basically lower than those observed after 04:54:14 UT except for a few points, at $\sim 04:49:24$, $\sim 04:51:55$, and $\sim 04:53:40$ UT. Although the fluxes were lower during 04:52:00–04:53:35 UT while B_x fluctuated around 0, the temperature was higher than those observed after 04:54:14 UT (blue trace in Figure 3g). Moreover, the magnetic field intensity was gradually declining from ~ 60 to ~ 40 nT (Figure 3d) as the spacecraft crossed the magnetopause. Based on the observations mentioned above, the spacecraft passed through from the region with the stronger magnetic field, lower density as well as higher temperature to the region with weaker magnetic field, higher density, and lower temperature. In other words, the spacecraft crossed the magnetopause from the Mercury's magnetosphere to the magnetosheath in the southern magnetopause, as shown in Figure 2. Since the IMF condition was nearly stable and northward, the magnetopause current sheet under such conditions can be investigated.

In the crossing of the magnetopause, B_y was very weak (< 10 nT) as B_x was less than -50 nT (before 04:52, and during 04:53:35–04:54:10 UT) whereas it fluctuated around 40 nT (Figure 3b) as $|B_x| < 30$ nT. It indicates that there was a nearly constant B_y component of ~ 40 nT inside the current sheet, 2 times stronger than B_y in the solar

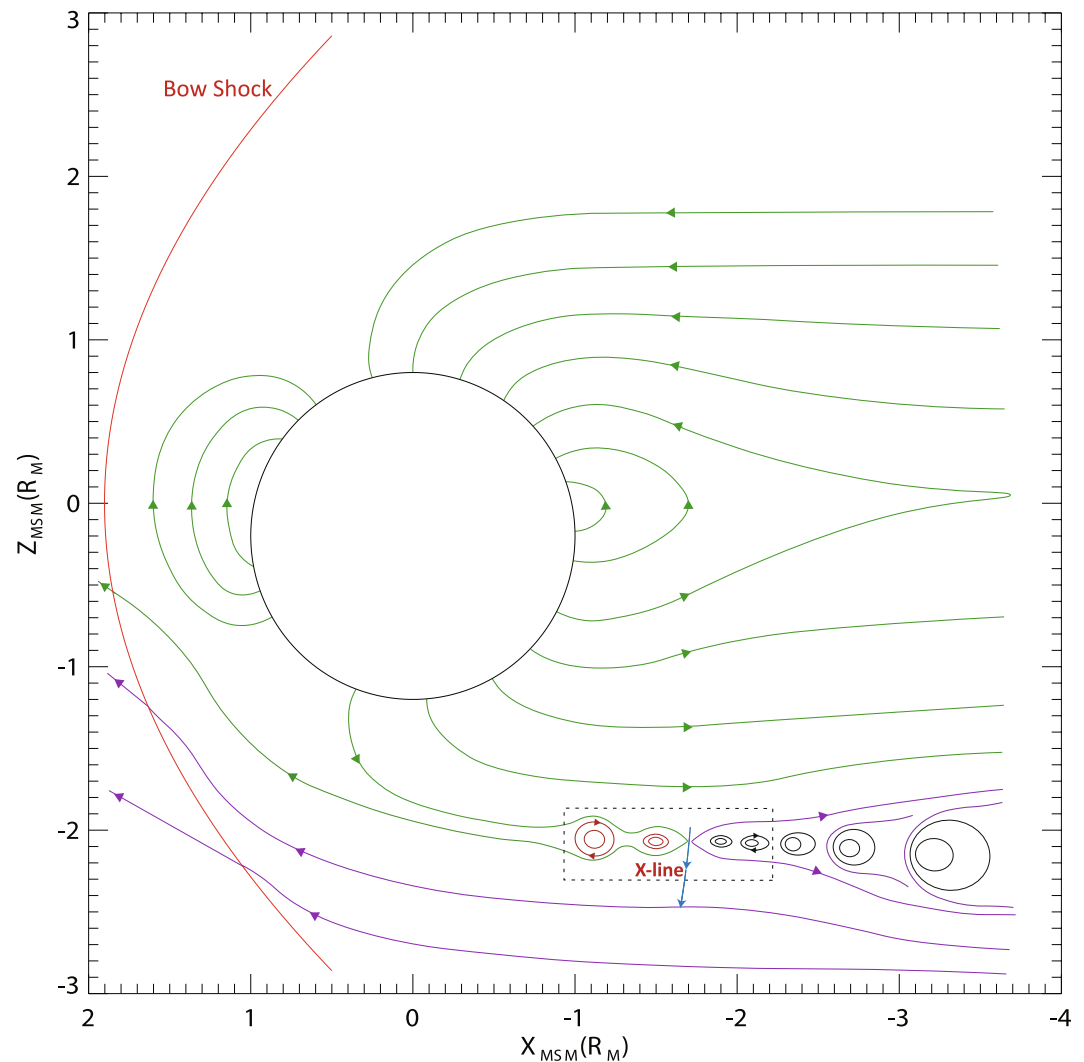


Figure 2. A schematic illustration of the Mercury's magnetosphere in the x - z plane of the Mercury Solar-Magnetospheric coordinates under the northern interplanetary magnetic field (IMF). The green and purple curves represent Mercury's and IMF lines. The bow shock is marked with a red curve. The dashed box denotes the observed X-line region, and the blue line with arrows represents the trace of the MErcury Surface Space ENvironment, GEochemistry, and Ranging spacecraft.

wind (Figure 1b). As the spacecraft passed through the current sheet, the average B_z (red trace in Figure 3c) varied from negative to positive roughly twice (between 04:48 and 04:53 UT, and between 04:53 and 04:58 UT), with a number of short bipolar B_z signatures which is supposed to be magnetic flux ropes and will be further studied later. The average B_z variation from negative to positive or vice versa inside the current sheet could correspond to the reconnected magnetic field at both outflow regions during magnetic reconnection. It indicates that the large-scale reconnection event was probably occurring at the high-latitude region of the southern magnetopause, and encountered by the spacecraft from one reconnection outflow to the other, as schematized in Figure 4f.

During the first reversal of the average B_z (04:51:10–04:52:10 UT, i.e., Region 0), B_x was basically negative at the reversal point (~04:51:50 UT), namely the spacecraft did not collect much data at the center of the reconnection X-line region. Here, we mainly focus on the second reversal of average B_z during 04:53:30–04:54:35 UT (Region 1), since B_x fluctuated around 0 in the vicinity of this B_z reversal point at 04:54:14 UT, where, as pointed out previously, the proton energy spectrum changed significantly. The proton pitch angle distribution was complicated in the magnetopause crossing (Figure 3f). After 04:54:14 UT, the flux enhancement was primarily observed nearly the direction perpendicular to the local magnetic field (~45° to ~110°) while the flux enhancement was

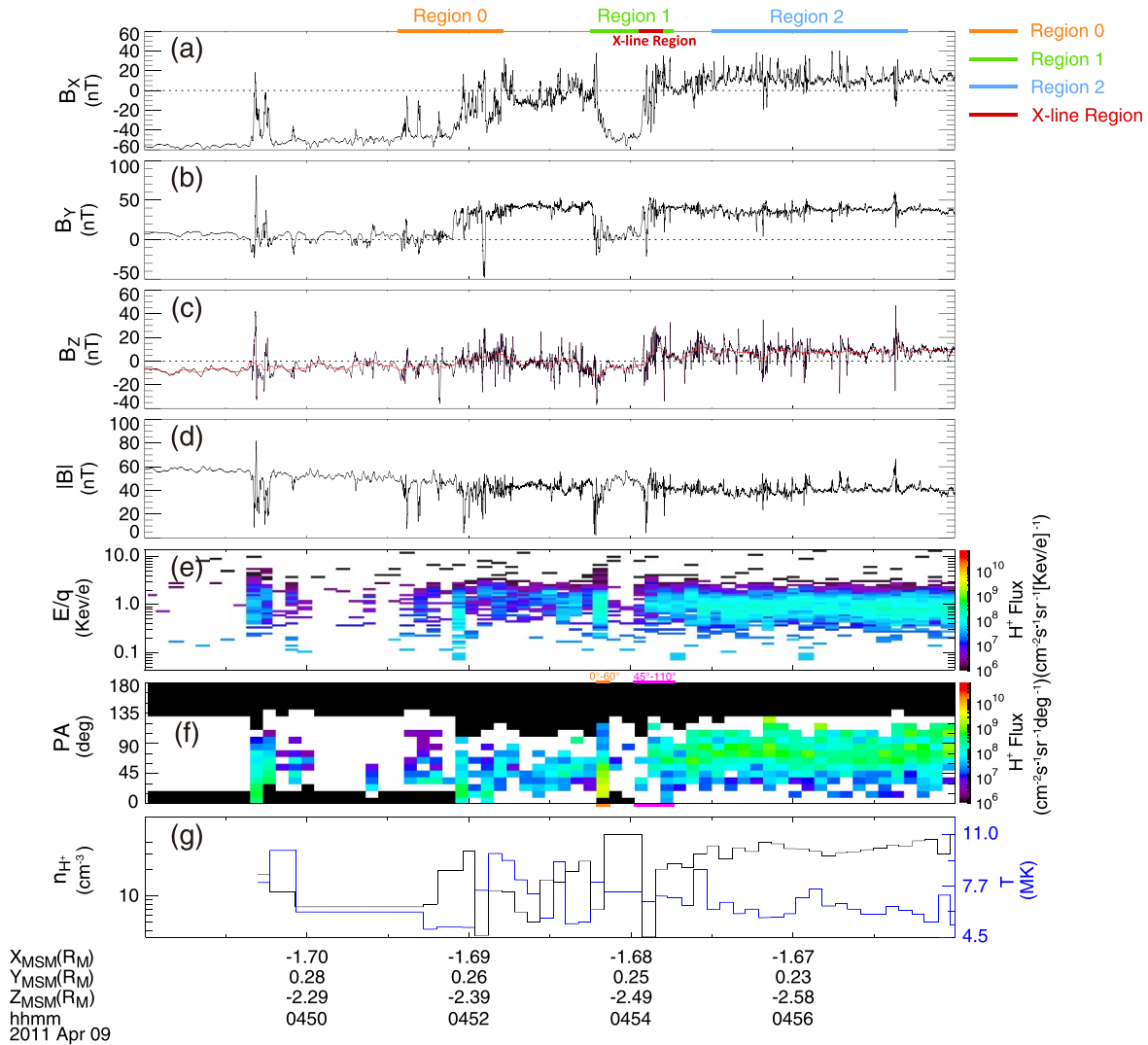


Figure 3. An overview of MErcury Surface Space ENvironment, GEochemistry, and Ranging's magnetopause current sheet crossing. (a–d) Magnetic field data (20 samples s^{-1}) in the Mercury Solar-Magnetospheric coordinate system. The red line in the panel (c) denotes the average B_z (1 s smoothed data). (e) Spectrogram of the proton differential energy flux versus energy per charge and time ($cm^{-2} Sr^{-2} S^{-1} [KeV/e]^{-1}$). (f) Pitch angle distribution of the proton differential energy flux versus degree and time ($cm^{-2} Sr^{-2} S^{-1} deg^{-1}$). (g) Proton number density (black triangles) and plasma temperature (blue circles). The orange, green, blue, and red horizontal lines at the top of the panel (a) denote Region 0 (04:51:05–04:52:10 UT), Region 1 (04:53:30–04:54:35 UT), Region 2 (04:55:00–04:57:30 UT), and X-line Region (04:54:07–04:54:23 UT), respectively.

detected nearly the parallel direction ($\sim 0^\circ$ to $\sim 60^\circ$) occasionally prior to 04:54:14 UT, for example, at $\sim 04:49:24$, $\sim 04:51:55$, $\sim 04:53:40$ UT (the orange horizontal bar in Figure 3f).

The magnetic field and the proton pitch angle distribution around the second reversal point of the average B_z , marked as “Region 1” at the top of Figure 3a, were further expanded in Figure 4a–4e. The minimum variance analysis (MVA) was performed on the magnetic field data during 04:53:40–04:54:40 UT to obtain the local current coordinate system (Sonnerup & Scheible, 1998), $L = [0.834, 0.517, 0.192]$, $M = [-0.537, 0.84, 0.073]$, and $N = [-0.124, -0.164, 0.979]$ relative to the MSM coordinates, and the eigenvalues are 923, 88, and 43. The ratio of maximum and intermediate eigenvalues is ~ 11 and the ratio of intermediate and minimum eigenvalues is ~ 2 . The MVA results did not alter too much if the time interval was adjusted.

Prior to the average B_N reversal point at $\sim 04:54:14$ UT, at least two short bipolar B_N signatures from positive to negative (the orange areas) were detected while the spacecraft was near the current sheet center at $\sim 04:53:33$ and $\sim 04:54:10$ UT (Figure 4a–4d). As for the first bipolar B_N signature, the curve in red, that is, the average \mathbf{B} which

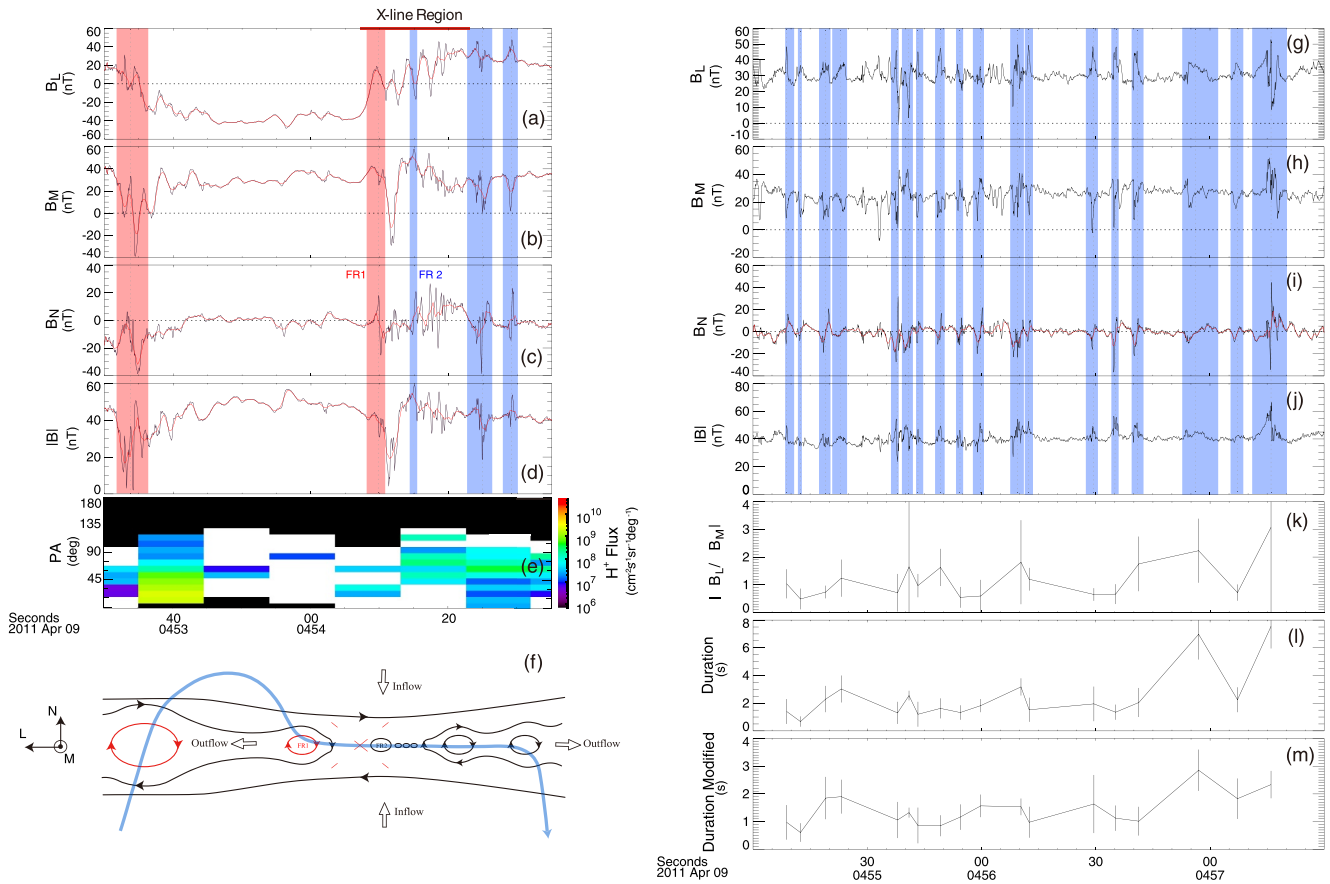


Figure 4. (a–d) Magnetic field data around the X-line region in the LMN coordinates. The orange and blue shadows marked the FRs with positive-to-negative and negative-to-positive B_N reversals, respectively. (e) Pitch angle distribution of proton flux versus degree and time. (f) A schematic for the reconnection site. (g–j) Three components and magnitude of Magnetic field. The blue shadows denote the flux ropes. (k) $|\Delta B_L/\Delta B_M|$, $\Delta B_M = B_{M_core} - B_{M_ave}$ where B_{M_core} denotes the average value of B_M between the minimum and maximum of B_N and B_{M_ave} is the 1 s average value of B_M before and after the flux rope boundary. If the time delay between two adjacent flux ropes was less than 1 s, B_{M_ave} was obtained by 1 s average value before the first one and after the second one. (l) The duration of each flux rope $T_{obse} = \frac{1}{2}(\Delta t_{max} + \Delta t_{min})$, where Δt_{max} is the time interval between the out boundary ($B_N = 0$) of flux ropes and Δt_{min} is the time span between the maximum and minimum of B_N . The errors are $\frac{1}{2}(\Delta t_{max} - \Delta t_{min})$. (m) The modified duration, calculated by the equation $T_{mod} = T_{obse} \times \left| \cos \left(\Delta B_M / \sqrt{\Delta B_M^2 + \Delta B_N^2} \right) \right|$.

can be regarded as the data in low-time resolution, shows a smooth evolution of B_N without sign change, accompanied with the minimum value of B_M and a peak of $|BI|$. It indicates that a large magnetic flux rope moving planetward was observed. This B_N bipolar signature was severely asymmetric due to a strong negative ambient B_N which could be from the reconnected magnetic field. The complex internal structure was observed within this flux rope (black curve). It looks like two short bipolar B_N signatures detected inside this large flux rope, analogous to previous observation in the Mercury's magnetotail (J. Zhong, Wei, et al., 2020) where this kind of magnetic field feature was thought to be a coalescence of magnetic flux ropes (Wang et al., 2016, 2017). Because of lack of the plasma data, we cannot confirm whether the coalescence of magnetic flux ropes was occurring here. For the second one, the bipolar B_N signature evolved smoothly with a small dip of B_M and $|BI|$ at its center (the vertical dashed line), consistent with crater magnetic flux rope frequently observed at the Earth's magnetopause (e.g., Hwang et al., 2020; C. Li et al., 2023; X. Li et al., 2023). These two bipolar B_N signatures were in good agreement with magnetic flux ropes moving planetward.

After the X-line region, another two bipolar B_N signatures from negative to positive were observed at $\sim 04:54:25$ UT and $\sim 04:54:29$ UT (the right two blue shadows in Figure 4a–4d). The one at $\sim 04:54:25$ UT exhibits a complex internal structure as well, while another one at $\sim 04:54:29$ UT shows a simple $|BI|$ peak. Thus, these two bipolar B_N signatures corresponded to two magnetic flux ropes moving tailward. Combining all these four magnetic flux ropes, the first two flux ropes were moving planetward whereas the last two were moving oppositely, tailward. It suggests that the middle region between these two groups of flux ropes should be their source region. Fortunately,

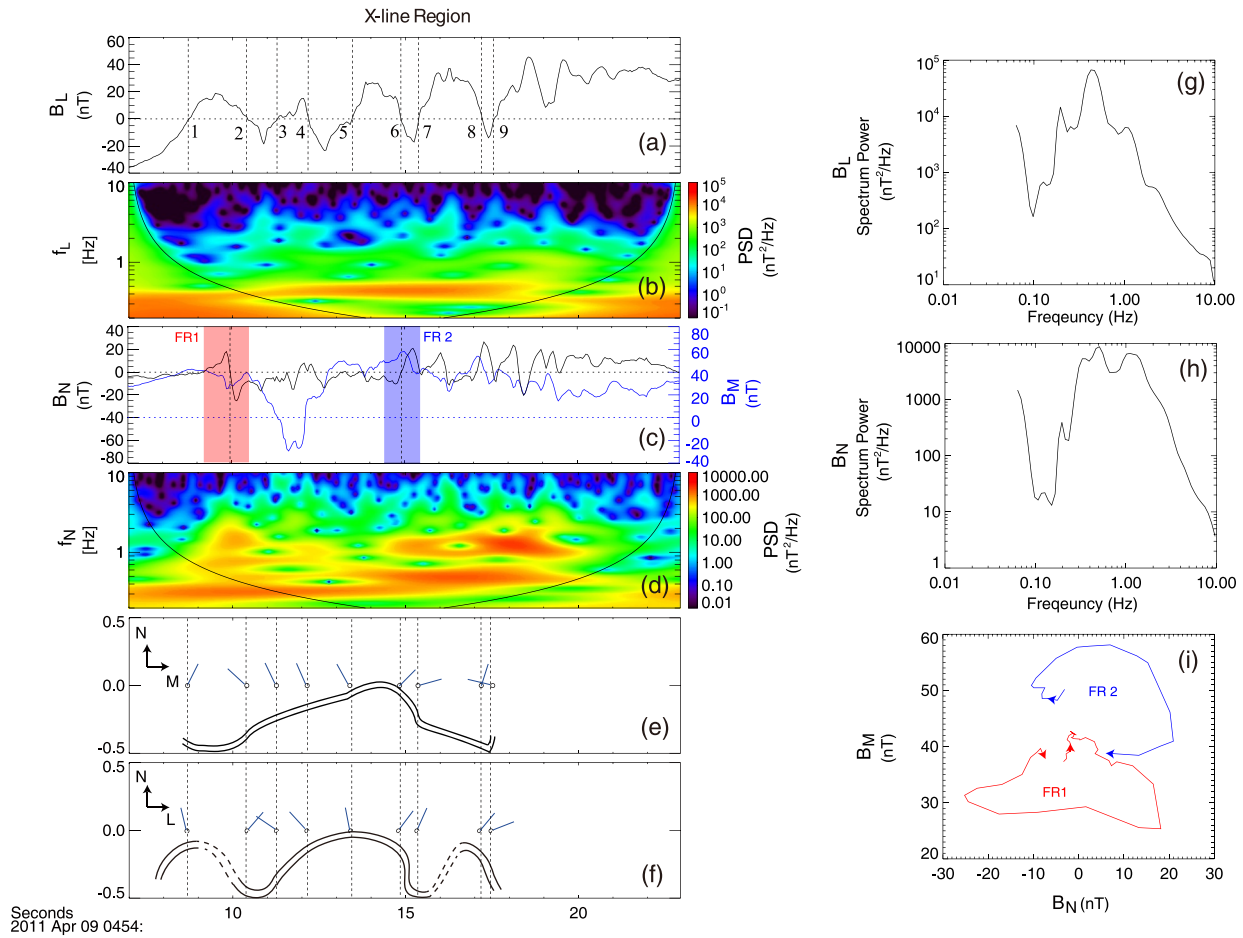


Figure 5. (a–f) Close-up view of the X-line Region. (a) B_L , the black dashed lines denote $B_L = 0$, labeled with 1–9. (b) Wavelet power spectral density (PSD) of B_L . (c) B_M (blue line) and B_N (black line). (d) Wavelet PSD of B_N . The areas below the black curve in panels (b) and (d) are the cone of influence regions. (e, f) The normal orientation of the current sheet displayed in M – N and L – N planes during each crossing. (g) and (h) Integrated power spectrum of B_L and B_N over the time span in panels (a)–(f). (i) Hodograms of B_M and B_N of FR1 and FR2 marked by red and blue shadows in panel (c).

B_L fluctuated around 0 in this region. Thus, the micro-physics inside this X-line region can be investigated in detail.

The short period of the X-line region (from 04:54:07 to 04:54:23 UT) is labeled by the red bar at the top of Figures 1a and 4a and enlarged in Figures 5a–5f. Within the X-line region, B_L displayed strong fluctuations with an amplitude of ~ 20 nT (Figure 5a) and B_N showed a similar variation (black curve in Figure 5c) as well. The wavelet analysis result of B_L and B_N shows clear frequency differences between them (Figures 5b, 5d, 5g, and 5h). The local wavelet power spectrum of B_L is mainly concentrated around 0.4 Hz (Figure 5b), consistent with the integrated wavelet spectrum where the power just peaks between 0.4 and 0.5 Hz (Figure 5g). For comparison, the wavelet analysis result of B_N is displayed in Figures 5d and 5h. The local power spectrum of B_N was enhanced in a broader frequency range from 0.2 to 2 Hz, identical to the integrated power spectrum in Figure 5h. This difference between the B_L and B_N fluctuations indicates that the fluctuations in these two directions could be attributed to different reasons.

The B_L sign change generally means a crossing of the current sheet (e.g., Shen et al., 2003). The strong B_L perturbation indicates that the current sheet in the X-line region was unstable and moving up and down. There were nine crossings of the current sheet identified and marked in Figure 5a. In these crossings, B_L varied from negative to positive or vice versa. The MVA method was employed to obtain the normal direction of each crossing in the local current coordinate system and the results are displayed in Table 1. Assuming that the normal direction always had a positive component in the N direction, we obtain its projections in the M – N (Figure 5e) and L – N

Table 1
Current Sheet Crossings in X-Line Region

Time ^a	Δt (s) ^b	CS normal in local coordinates	λ_1/λ_2	λ_2/λ_3
04:54:08.751	2.50	[−0.210, 0.438, 0.874]	67.22	5.41
04:54:10.451	0.70	[0.511, −0.632, 0.582]	5.78	9.93
04:54:11.301	1.10	[−0.802, −0.258, 0.539]	10.17	5.55
04:54:12.201	0.60	[−0.648, −0.305, 0.698]	8.80	5.28
04:54:13.451	1.05	[−0.167, −0.477, 0.863]	10.13	9.57
04:54:14.851	1.40	[0.476, 0.618, 0.626]	8.68	8.98
04:54:15.401	1.70	[0.120, 0.956, 0.267]	6.79	20.49
04:54:17.201	1.05	[0.626, 0.235, 0.744]	9.18	7.29
04:54:17.551	0.35	[0.512, −0.836, 0.198]	6.75	5.04

^aThe time of the current sheet crossing defined by when $B_L = 0$. ^bThe interval for performing MVA analysis.

(Figure 5f) planes. Because of the average B_z reversal point at ~04:54:14 UT (i.e., the X-line), the first five crossings labeled as “1”–“5” were detected in the planetward outflow region while the left four crossings (the crossings “6”–“9”) happened in the tailward outflow region. The crossings 2–5 exhibited a negative M component in the planetward outflow region while the crossings 6–8 showed a positive M component. It looks like the local current layer at the X-line was bent, as illustrated in Figure 5e, which can be found also in the L – N plane (Figure 5f). On the other hand, there could be much smaller scale variation in the L component, as shown in the L – N plane, which could be related to the B_N variation.

Inside the X-line region, the magnetic flux rope at 04:54:10UT, was identified previously to be moving planetward, now named FR1. Near the center of the X-line region, another small-scale flux rope at 04:54:15 UT was discerned according to the bipolar B_N signature and a B_M peak at its center (blue curve in Figure 5c), named FR2. A clear rotation of the magnetic field in the hodogram of these two flux ropes was evident (Figure 5i). It further supports that the observed bipolar signatures inside the X-line region were identical to mag-

netic flux ropes which could be due to the newborn small-scale magnetic flux ropes inside the reconnection diffusion region, as observed previously and named as “secondary flux rope” (e.g., Eastwood et al., 2007; Wang et al., 2010, 2016; J. Zhong et al., 2018; Z. H. Zhong et al., 2018).

After the reconnection X-line region, large amounts of flux ropes were detected one after another, characterized by a bipolar B_z and coincident enhancement of $|B|$ (Figure 3). An interval (labeled as Region 2 at the top of Figure 3) of these bipolar B_z signatures was expanded in Figure 4g–4j and displayed in the local current coordinate system. All these bipolar B_N varied from negative to positive (blue shadow in Figure 4i) except for the last one at ~04:57:16 UT, namely, they were ejected away from the X-line toward the Mercury’s magnetotail (Figure 2). In the local current coordinates, the ambient magnetic field of B_N was close to 0. Therefore, there were three points of $B_N = 0$ during each bipolar B_N signature. The two outer points of $B_N = 0$ were defined as the boundaries of one flux rope, as the blue bars in Figure 4i and its duration is t_{\max} . The point of $B_N = 0$ in the middle was defined as the center of the flux rope (the vertical dashed line). The area between the minimum and maximum of each bipolar B_N was the core region of each flux rope and its duration was t_{\min} . Figure 4i shows the duration of each flux rope $T_{\text{obse}} = \frac{1}{2}(\Delta t_{\max} + \Delta t_{\min})$ and the error bar is $\frac{1}{2}(\Delta t_{\max} - \Delta t_{\min})$. The duration of most flux ropes was about 2 s and the longest was ~7 s at ~04:56:57 and ~04:57:15 UT. The two longest flux ropes were observed farthest away from the x-line region. As for the last flux rope at ~04:57:16 UT, there were several points of $B_N = 0$. Thus, the average data (1 s smoothed data, red trace in Figure 4j) were used to identify the flux rope and its duration.

In general, B_M peaked inside the flux rope and the M direction is regarded as the axis direction (e.g., Cowley, 1982; Eastwood et al., 2012; Hara et al., 2017; Slavin et al., 2003). In our event, however, the B_L peaks were detected in most of the flux ropes rather than the expected B_M , and the B_M peak was only observed in a few flux ropes (Figures 4g and 4h). Simultaneously, $|B|$ always peaked at these flux ropes. It indicates that the axes of most flux ropes here might be deflected away from the M direction to the L direction. The flux rope deflection was not observed in the outflow toward the planet but was clear in the tailward outflow region.

Since the average value of B_N was around 0 in the core region, the magnetic field was primarily in the L – M plane. Thus, $|\Delta B_L|/|\Delta B_M|$ within the core region of each flux rope in Figure 4k was used to quantify the deflection, where ΔB_L and ΔB_M are the perturbation field (see the caption in Figure 4). The larger value of $|\Delta B_L|/|\Delta B_M|$ represents more deflective away from the M direction to the L direction. The values of $|\Delta B_L|/|\Delta B_M|$ were from 0.5 to 3. It means that the flux ropes in the reconnection tailward outflow were probably deflected significantly. Moreover, the values of $|\Delta B_L|/|\Delta B_M|$ had a tendency to increase over time. In other words, it is possible that the flux ropes were deflected more as they were moving further away from the reconnection X-line.

The duration roughly represented the cross-section scale of one flux rope. Since the flux rope was deflected substantially, the observed duration cannot accurately represent the size of the cross-section. In order to eliminate this effect, the duration was further modified by the equation $T_{\text{mod}} = T_{\text{obse}} \times \left| \cos \left(\Delta B_M / \sqrt{\Delta B_M^2 + \Delta B_L^2} \right) \right|$ which

was shown in Figure 4m. In the tailward reconnection outflow, the flux ropes encountered by the spacecraft later were further away from the reconnection X-line if the X-line was moving planetward. On average, the duration increased as the flux ropes were observed further away from the reconnection X-line. Thus, the observations suggested that the flux ropes were expanding as they propagated away from the X-line. We had to point out that the spacecraft trajectory relative to the flux rope center could also affect our result. Currently, this effect has not been taken into account. Based on the analysis above, it seems that the flux ropes moving tailward were significantly deflected away from the M direction. As these flux ropes were ejected away from the X-line region, they were expanding gradually.

3. Discussion and Conclusions

Magnetic reconnection is believed to control the coupling between the solar wind and Mercury's magnetosphere under the condition of the southward IMF (e.g., Slavin et al., 2008). Based on the MESSENGER measurements, the magnetic reconnection signatures have been extensively observed, including magnetic flux ropes, magnetic islands, and traveling compressing regions. In particular, a train of magnetic flux ropes is frequently observed in the Mercury's magnetotail and magnetopause, dubbed flux rope shower (Slavin, Imber, et al., 2012; Sun, Slavin, Smith, et al., 2020; J. Zhong, Wei, et al., 2020), and is supposed to be produced by reconnection occurring simultaneously at multiple points. However, the properties of reconnection X-line region have never been in situ measured in Mercury's magnetosphere so far, although the Hall magnetic field was detected recently in the reconnection events (Sun, Slavin, Smith, et al., 2020; J. Zhong, Wei, et al., 2020).

In this letter, we observed an ongoing magnetic reconnection at the south magnetopause. This ongoing reconnection event was moving toward Mercury and passed the spacecraft. Therefore, the spacecraft observed magnetic flux ropes propagating planetward at first and then the flux ropes moving away from Mercury. Between the two groups of flux ropes moving toward and away from Mercury, the spacecraft crossed the current sheet multiple times. Namely, the spacecraft encountered the current sheet in the X-line region. The current sheet is distorted, especially in the L - N plane. Within the current sheet, a series of bipolar B_N was detected continuously. These bipolar B_N could be newborn small-scale magnetic flux ropes and then were ejected away from the X-line region. This could be the reason why so many magnetic flux ropes, that is, the flux rope shower, were observed in Mercury's magnetopause.

The flux rope shower has been successfully realized recently in the three-dimensional global hybrid simulations under both northward and southward IMF conditions (Lu, Guo, et al., 2022). During the northward IMF, the flux ropes are repeatedly generated in the limited region at the high-latitude magnetopause and then leave away at a high speed, which is in good agreement with our speculation. In the high-latitude magnetopause, the tailward plasma flow in which these flux tubes are embedded would be super-Alfvénic and the density and temperature asymmetry would be significant across it, which possibly leads to reconnection suppression (e.g., Liu & Hesse, 2016; Swisdak et al., 2003) and thus exclude the scenario of multiple X-line reconnection therein.

After the flux ropes were ejected away from the X-line region, they probably expanded and significantly tilted away from the M direction. The evolution of the generated flux ropes has not been revealed so far by in situ observation. However, the flux rope expansion can be clearly found in Figure 5 of the hybrid simulations (Lu, Guo, et al., 2022) and in Figure 3 of the Hall MHD simulations (C. Li et al., 2023; X. Li et al., 2023). The expansion of the flux rope could be the reason why the large-scale magnetic flux rope was detected in Mercury's magnetosphere (Imber et al., 2014; Slavin et al., 2010). The resulting effect on Mercury's magnetosphere dynamics remains unclear.

Under the condition of the northward IMF, a total of 163 FTEs were detected tailward of Mercury's southern magnetic cusp and they had elliptical cross-sections with a mean semimajor axis of 0.15 Mercury's radius and a mean axial magnetic flux of 1.25 MWb (Slavin, Imber, et al., 2012). The reconnection near or just tailward of the southern cusp did not add or subtract any net magnetic flux from the magnetotail. This reconnection stripped the open magnetic field lines out of the magnetotail lobes tailward of the X-line and added to the lobes planetward of the X-line magnetic field lines carrying the magnetosheath plasma. Therefore, the flux ropes tailward of the X-line were an interplanetary flux tube as both ends were pulled by the solar wind and were driven downstream by the curvature force from the hairpin magnetic field configuration (Figure 2). In contrast, the smaller flux ropes planetward of the X-line hold the open flux tubes connecting the upstream solar wind to the near-tail. The evolution of these smaller flux ropes moving toward Mercury was complicated and could be controlled by many

impacts. The dynamics of the Mercury's magnetosphere configuration in the northward IMF condition is still open and needs to be modeled further with numerical simulations.

In summary, we present one ongoing reconnection event at the high-latitude magnetopause under the condition of the north IMF. The reconnection site was approaching Mercury and thus the spacecraft crossed the reconnection X-line region from the planetward outflow region to the tailward outflow region. In the X-line region, a few small magnetic flux ropes were detected which could be the source of the large flux ropes observed at the magnetopause. After being ejected away from the X-line region, these flux ropes probably expanded and were significantly tilted away from the M direction in the tailward reconnection outflow.

Data Availability Statement

The magnetic field data (Anderson et al., 2007) on which this paper is based are available on the website at <https://pds-ppi.igpp.ucla.edu/search/view/?f=yes&id=pds://PPI/mess-mag-calibrated/data>, and the plasma data (Andrews et al., 2007) can be found in the website of <https://pds-ppi.igpp.ucla.edu/search/view/?f=yes&id=pds://PPI/mess-epps-fips-calibrated>.

Acknowledgments

This research was funded by the B-type Strategic Priority Program of the Chinese Academy of Sciences (XDB41000000), the National Science Foundation of China (NSFC) Grant 42174181, Key Research Program of Frontier Sciences CAS (QYZDJ-SSW-DQC010).

References

- Alexeev, I. I., Belenkaya, E. S., Slavin, J. A., Korth, H., Anderson, B. J., Baker, D. N., et al. (2010). Mercury's magnetospheric magnetic field after the first two MESSENGER flybys. *Icarus*, 209(1), 23–39. <https://doi.org/10.1016/j.icarus.2010.01.024>
- Anderson, B. J., Acuña, M. H., Korth, H., Purucker, M. E., Johnson, C. L., Slavin, J. A., et al. (2008). The structure of Mercury's magnetic field from MESSENGER's first flyby. *Science*, 321(5885), 82–85. <https://doi.org/10.1126/science.1159081>
- Anderson, B. J., Acuña, M. H., Lohr, D. A., Scheifele, J., Raval, A., Korth, H., & Slavin, J. A. (2007). The magnetometer instrument on MESSENGER. *Space Science Reviews*, 131(1), 417–450. <https://doi.org/10.1007/s11214-007-9246-7>
- Anderson, B. J., Johnson, C. L., Korth, H., Purucker, M. E., Winslow, R. M., Slavin, J. A., et al. (2011). The global magnetic field of Mercury from MESSENGER orbital observations. *Science*, 333(6051), 1859–1862. <https://doi.org/10.1126/science.1211001>
- Andrews, G. B., Zurbuchen, T. H., Mauk, B. H., Malcom, H., Fisk, L. A., Gloeckler, G., et al. (2007). The energetic particle and plasma spectrometer instrument on the MESSENGER spacecraft. *Space Science Reviews*, 131(1), 523–556. <https://doi.org/10.1007/s11214-007-9272-5>
- Chen, L. J., Bhattacharjee, A., Puhl-Quinn, P., Yang, H., Bessho, N., Imada, S., et al. (2008). Observation of energetic electrons within magnetic islands. *Nature Physics*, 4(1), 19–23. <https://doi.org/10.1038/nphys777>
- Cowley, S. W. H. (1982). The causes of convection in the Earth's magnetosphere: A review of developments during the IMS. *Reviews of Geophysics*, 20(3), 531–565. <https://doi.org/10.1029/RG020i003p00531>
- DiBraccio, G. A., Slavin, J. A., Imber, S. M., Gershman, D. J., Raines, J. M., Jackman, C. M., et al. (2015). MESSENGER observations of flux ropes in Mercury's magnetotail. *Planetary and Space Science*, 115, 77–89. <https://doi.org/10.1016/j.pss.2014.12.016>
- Eastwood, J. P., Phan, T. D., Mozer, F. S., Shay, M. A., Fujimoto, M., Retino, A., et al. (2007). Multi-point observations of the Hall electromagnetic field and secondary island formation during magnetic reconnection. *Journal of Geophysical Research*, 112(A6), A06235. <https://doi.org/10.1029/2006ja012158>
- Eastwood, J. P., Videira, J. J. H., Brain, D. A., & Halekas, J. S. (2012). A chain of magnetic flux ropes in the magnetotail of Mars. *Geophysical Research Letters*, 39(3), 524. <https://doi.org/10.1029/2011GL050444>
- Gershman, D. J., Dorelli, J. C., DiBraccio, G. A., Raines, J. M., Slavin, J. A., Poh, G., & Zurbuchen, T. H. (2016). Ion-scale structure in Mercury's magnetopause reconnection diffusion region. *Geophysical Research Letters*, 43(12), 5935–5942. <https://doi.org/10.1002/2016gl069163>
- Gershman, D. J., Slavin, J. A., Raines, J. M., Zurbuchen, T. H., Anderson, B. J., Korth, H., et al. (2013). Magnetic flux pileup and plasma depletion in Mercury's subsolar magnetosheath. *Journal of Geophysical Research: Space Physics*, 118(11), 7181–7199. <https://doi.org/10.1002/2013JA019244>
- Gershman, D. J., Zurbuchen, T. H., Fisk, L. A., Gilbert, J. A., Raines, J. M., Anderson, B. J., et al. (2012). Solar wind alpha particles and heavy ions in the inner heliosphere observed with MESSENGER. *Journal of Geophysical Research*, 117(A12), A00M02. <https://doi.org/10.1029/2012JA017829>
- Guo, J., Lu, S., Lu, Q., Lin, Y., Wang, X., Huang, K., et al. (2021). Structure and coalescence of magnetopause flux ropes and their Dependence on IMF clock angle: Three-dimensional global hybrid simulations. *Journal of Geophysical Research: Space Physics*, 126(2), e2020JA028670. <https://doi.org/10.1029/2020ja028670>
- Hara, T., Harada, Y., Mitchell, D. L., DiBraccio, G. A., Espley, J. R., Brain, D. A., et al. (2017). On the origins of magnetic flux ropes in near-Mars magnetotail current sheets. *Geophysical Research Letters*, 44(15), 7653–7662. <https://doi.org/10.1002/2017GL073754>
- Hwang, K. J., Dokgo, K., Choi, E., Burch, J. L., Sibeck, D. G., Giles, B. L., et al. (2020). Magnetic reconnection inside a flux rope induced by Kelvin-Helmholtz vortices. *Journal of Geophysical Research: Space Physics*, 125(4), e2019JA027665. <https://doi.org/10.1029/2019JA027665>
- Imber, S. M., Slavin, J. A., Boardsen, S. A., Anderson, B. J., Korth, H., McNutt, R. L., Jr., & Solomon, S. C. (2014). MESSENGER observations of large dayside flux transfer events: Do they drive Mercury's substorm cycle? *Journal of Geophysical Research: Space Physics*, 119(7), 5613–5623. <https://doi.org/10.1002/2014ja019884>
- Jia, X., Slavin, J. A., Poh, G., DiBraccio, G. A., Toth, G., Chen, Y., et al. (2019). MESSENGER observations and global simulations of highly compressed magnetosphere events at Mercury. *Journal of Geophysical Research: Space Physics*, 124(1), 229–247. <https://doi.org/10.1029/2018ja026166>
- Lee, L. C., & Fu, Z. F. (1985). A theory of magnetic flux transfer at the Earth's magnetopause. *Geophysical Research Letters*, 12(2), 105–108. <https://doi.org/10.1029/gl012i002p00105>
- Li, C., Jia, X., Chen, Y., Toth, G., Zhou, H., Slavin, J. A., et al. (2023). Global Hall MHD simulations of Mercury's magnetopause dynamics and FTEs under different solar wind and IMF conditions. *Journal of Geophysical Research: Space Physics*, 128(5), e2022JA031206. <https://doi.org/10.1029/2022ja031206>

- Li, X., Wang, R., & Lu, Q. (2023). Division of magnetic flux rope via magnetic reconnection observed in the magnetotail. *Geophysical Research Letters*, *50*(1), e2022GL101084. <https://doi.org/10.1029/2022GL101084>
- Liu, Y. H., & Hesse, M. (2016). Suppression of collisionless magnetic reconnection in asymmetric current sheets. *Physics of Plasmas*, *23*(6), 060704. <https://doi.org/10.1063/1.4954818>
- Lu, Q., Fu, H. S., Wang, R. S., & Lu, S. (2022). Collisionless magnetic reconnection in the magnetosphere. *Chinese Physics B*, *31*(8), 089401. <https://doi.org/10.1088/1674-1056/ac76ab>
- Lu, Q., Guo, J., Lu, S., Wang, X., Slavin, J. A., Sun, W., et al. (2022). Three-dimensional global hybrid simulations of flux transfer event showers at Mercury. *The Astrophysical Journal*, *937*(1), 1. <https://doi.org/10.3847/1538-4357/ac8bcf>
- Rijnbeek, R. P., Cowley, S. W. H., Southwood, D. J., & Russell, C. T. (1984). A survey of dayside flux transfer events observed by ISEE 1 and 2 magnetometers. *Journal of Geophysical Research*, *89*(A2), 786–800. <https://doi.org/10.1029/ja089ia02p00786>
- Russell, C. T., & Elphic, R. C. (1978). Initial ISEE magnetometer results: Magnetopause observations. *Space Science Reviews*, *22*(6), 681–715. <https://doi.org/10.1007/bf00212619>
- Shen, C., Li, X., Dunlop, M., Liu, Z. X., Balogh, A., Baker, D. N., et al. (2003). Analyses on the geometrical structure of magnetic field in the current sheet based on cluster measurements. *Journal of Geophysical Research*, *108*(A5), 1168. <https://doi.org/10.1029/2002JA009612>
- Slavin, J. A., Acuña, M. H., Anderson, B. J., Baker, D. N., Benna, M., Gloeckler, G., et al. (2008). Mercury's magnetosphere after MESSENGER's first flyby. *Science*, *321*(5885), 85–89. <https://doi.org/10.1126/science.1159040>
- Slavin, J. A., Anderson, B. J., Baker, D. N., Benna, M., Boardsen, S. A., Gold, R. E., et al. (2012). MESSENGER and Mariner 10 flyby observations of magnetotail structure and dynamics at Mercury. *Journal of Geophysical Research*, *117*(A1), E00L14. <https://doi.org/10.1029/2011JA016900>
- Slavin, J. A., DiBraccio, G. A., Gershman, D. J., Imber, S. M., Poh, G. K., Raines, J. M., et al. (2014). MESSENGER observations of Mercury's dayside magnetosphere under extreme solar wind conditions. *Journal of Geophysical Research: Space Physics*, *119*(10), 8087–8116. <https://doi.org/10.1002/2014ja020319>
- Slavin, J. A., & Holzer, R. E. (1979). The effect of erosion on the solar wind stand-off distance at Mercury. *Journal of Geophysical Research*, *84*(A5), 2076–2082. <https://doi.org/10.1029/ja084ia05p02076>
- Slavin, J. A., Imber, S. M., Boardsen, S. A., DiBraccio, G. A., Sundberg, T., Sarantos, M., et al. (2012). MESSENGER observations of a flux-transfer-event shower at Mercury. *Journal of Geophysical Research*, *117*(A12), A00M06. <https://doi.org/10.1029/2012JA017926>
- Slavin, J. A., Lepping, R. P., Gjerloev, J., Fairfield, D. H., Hesse, M., Owen, C. J., et al. (2003). Geotail observations of magnetic flux ropes in the plasma sheet. *Journal of Geophysical Research*, *108*(A1), SMP10-11–SMP10-18. <https://doi.org/10.1029/2002JA009557>
- Slavin, J. A., Lepping, R. P., Wu, C., Anderson, B. J., Baker, D. N., Benna, M., et al. (2010). MESSENGER observations of large flux transfer events at Mercury. *Geophysical Research Letters*, *37*(2), L02105. <https://doi.org/10.1029/2009gl041485>
- Sonnerup, B. U. Ö., & Scheible, M. (1998). Minimum and maximum variance analysis. *ISSI Scientific Reports Series*, *1*, 185–220.
- Sun, W. J., Dewey, R. M., Aizawa, S., Huang, J., Slavin, J. A., Fu, S., et al. (2022). Review of Mercury's dynamic magnetosphere: Post MESSENGER era and comparative magnetospheres. *Science China Earth Sciences*, *65*(1), 25–74. <https://doi.org/10.1007/s11430-021-9828-0>
- Sun, W. J., Slavin, J. A., Dewey, R. M., Chen, Y., DiBraccio, G. A., Raines, J. M., et al. (2020). MESSENGER observations of Mercury's nightside magnetosphere under extreme solar wind conditions: Reconnection-generated structures and steady convection. *Journal of Geophysical Research: Space Physics*, *125*(3), e2019JA027490. <https://doi.org/10.1029/2019ja027490>
- Sun, W.-J., Slavin, J. A., Fu, S., Raines, J. M., Zong, Q., Imber, S. M., et al. (2015). MESSENGER observations of magnetospheric substorm activity in Mercury's near magnetotail. *Geophysical Research Letters*, *42*(10), 3692–3699. <https://doi.org/10.1002/2015gl064052>
- Sun, W. J., Slavin, J. A., Smith, A. W., Dewey, R. M., Poh, G. K., Jia, X., et al. (2020). Flux transfer event showers at Mercury: Dependence on plasma β and magnetic shear and their contribution to the Dungey cycle. *Geophysical Research Letters*, *47*(21), e2020GL089784. <https://doi.org/10.1029/2020gl089784>
- Swisdak, M., Rogers, B. N., Drake, J. F., & Shay, M. A. (2003). Diamagnetic suppression of component magnetic reconnection at the magnetopause. *Journal of Geophysical Research*, *108*(A5), 1218. <https://doi.org/10.1029/2002ja009726>
- Wang, R., Lu, Q., Du, A., & Wang, S. (2010). In situ observations of a secondary magnetic island in an ion diffusion region and associated energetic electrons. *Physical Review Letters*, *104*(17), 175003. <https://doi.org/10.1103/physrevlett.104.175003>
- Wang, R., Lu, Q., Nakamura, R., Baumjohann, W., Russell, C. T., Burch, J. L., et al. (2017). Interaction of magnetic flux ropes via magnetic reconnection observed at the magnetopause. *Journal of Geophysical Research: Space Physics*, *122*(10), 10436–10447. <https://doi.org/10.1002/2017ja024482>
- Wang, R., Lu, Q., Nakamura, R., Huang, C., Du, A., Guo, F., et al. (2016). Coalescence of magnetic flux ropes in the ion diffusion region of magnetic reconnection. *Nature Physics*, *12*(3), 263–267. <https://doi.org/10.1038/nphys3578>
- Wang, R., Nakamura, R., Lu, Q., Du, A., Zhang, T., Baumjohann, W., et al. (2012). Asymmetry in the current sheet and secondary magnetic flux ropes during guide field magnetic reconnection. *Journal of Geophysical Research*, *117*(A7), 10436–10447. <https://doi.org/10.1029/2011ja017384>
- Zhong, J., Lee, L. C., Wang, X. G., Pu, Z. Y., He, J. S., Wei, Y., & Wan, W. X. (2020). Multiple X-line reconnection observed in Mercury's magnetotail driven by an interplanetary coronal mass ejection. *The Astrophysical Journal Letters*, *893*(1), L11. <https://doi.org/10.3847/2041-8213/ab8380>
- Zhong, J., Wei, Y., Lee, L. C., He, J. S., Slavin, J. A., Pu, Z. Y., et al. (2020). Formation of macroscale flux transfer events at Mercury. *The Astrophysical Journal Letters*, *893*(1), L18. <https://doi.org/10.3847/2041-8213/ab8566>
- Zhong, J., Wei, Y., Pu, Z. Y., Wang, X. G., Wan, W. X., Slavin, J. A., et al. (2018). MESSENGER observations of rapid and impulsive magnetic reconnection in Mercury's magnetotail. *The Astrophysical Journal Letters*, *860*(2), L20. <https://doi.org/10.3847/2041-8213/aaca92>
- Zhong, Z. H., Tang, R. X., Zhou, M., Deng, X. H., Pang, Y., Paterson, W. R., et al. (2018). Evidence for secondary flux rope generated by the electron Kelvin-Helmholtz instability in a magnetic reconnection diffusion region. *Physical Review Letters*, *120*(7), 075101. <https://doi.org/10.1103/physrevlett.120.075101>
- Zomerdijsk-Russell, S., Masters, A., Sun, W. J., Fear, R. C., & Slavin, J. A. (2023). Does reconnection only occur at points of maximum shear on Mercury's dayside magnetopause? *Journal of Geophysical Research: Space Physics*, *128*(11), e2023JA031810. <https://doi.org/10.1029/2023ja031810>